Physics of Fluids

Large-scale clustering of light small particles in developed turbulence

Cite as: Phys. Fluids **33**, 031707 (2021); https://doi.org/10.1063/5.0041873
Submitted: 26 December 2020 . Accepted: 06 February 2021 . Published Online: 17 March 2021

Sunao Oka (岡温), Daiki Watanabe (渡邊大記), and Susumu Goto (後藤晋)

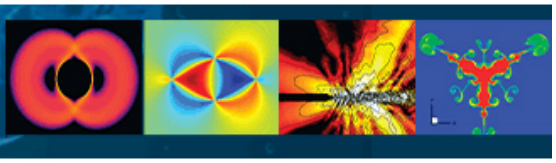

Physics of Fluids LETTER scitation.org/journal/phf

Large-scale clustering of light small particles in developed turbulence

Cite as: Phys. Fluids **33**, 031707 (2021); doi: 10.1063/5.0041873
Submitted: 26 December 2020 · Accepted: 6 February 2021 ·
Published Online: 17 March 2021

View Online Export Citation CrossMark

Sunao Oka (岡温),[a] Daiki Watanabe (渡邊大記), and Susumu Goto (後藤晋)[a]

AFFILIATIONS

Graduate School of Engineering Science, Osaka University, 1-3 Machikaneyama, Toyonaka, Osaka 560-8531, Japan

[a]Author to whom correspondence should be addressed: s_oka@fm.me.es.osaka-u.ac.jp and goto@me.es.osaka-u.ac.jp

ABSTRACT

Small solid particles, droplets, and bubbles can form clusters in turbulent flows by the action of coherent vortices. This phenomenon, sometimes called the preferential concentration, was often thought to be most conspicuous when the velocity relaxation time τ_p of particles is comparable with the Kolmogorov time τ_η. However, since high-Reynolds number turbulence consists of coherent eddies with different timescales, particles can form clusters even when $\tau_p \gg \tau_\eta$. We demonstrate, by direct numerical simulations, that light particles with different τ_p values form clusters around axes of coherent vortices with different sizes in developed turbulence.

Despite the strong mixing ability of turbulent flows, small particles can be unmixed to form clusters in turbulence[1,2] if particles and fluid have different mass densities. This interesting phenomenon has been attracting researchers in various fields. In fact, many authors extensively investigated the behavior of small heavy particles in turbulence because it is relevant to the droplet growth in cloud turbulence,[3–5] the formation of planets,[6,7] the pattern formation of river beds,[8,9] and so on. Several mechanisms[10–20] were proposed to explain the clustering of particles in turbulence. Among them, the most fundamental one[10–13] is the mechanism by the action of coherent eddies in the Kolmogorov length η; since heavy particles around an eddy cannot acquire sufficient centripetal force by the pressure gradient of fluid, they are swept out from the eddy to accumulate in high-strain rate regions around it. This classical mechanism is the starting point of the present study. On the other hand, we often use small light particles, such as air bubbles in water, for the visualization of vortices in laboratory experiments (see, for example, Ref. 21). This implies that light particles form clusters around the axis of vortices. Although this phenomenon is well known and some recent studies[22–24] dealt with it, the systematic study of small light particles in turbulence is rather limited.

Recent powerful numerical simulations have revealed that there exists a hierarchy of coherent vortices with different sizes in high-Reynolds number turbulence.[25–27] This multi-scale nature implies that turbulence has various timescales, which is important for particle motions. Since particles tend to follow flow with a finite time lag, i.e., the velocity relaxation time τ_p [see (3), below], the clusters of small particles can be different depending on τ_p due to the multi-scale nature of turbulence. In fact, small heavy particles accumulate in the straining regions between the vortices whose turnover time is comparable to τ_p.[16,18,28]

The purpose of the present study is to show that light particles with different τ_p values also form clusters around the axis of vortices with different sizes; in particular, the clusters can be much larger than the Kolmogorov scale in developed turbulence. In the following, we demonstrate this by direct numerical simulations (DNSs) and explain the observed phenomenon by simple physical arguments.

We investigate the behavior of small particles in turbulence of an incompressible fluid. Although here we consider turbulence in a periodic cube with the period being 2π, the following arguments are independent of the boundary condition. Let $\boldsymbol{u}(\boldsymbol{x},t)$ and $p(\boldsymbol{x},t)$ be the velocity and pressure of fluid at position $\boldsymbol{x}$ and time t. The Navier-Stokes equation, $\partial\boldsymbol{u}/\partial t + \boldsymbol{u}\cdot\nabla\boldsymbol{u} = -(1/\rho_f)\nabla p + \nu\nabla^2\boldsymbol{u} + \boldsymbol{f}$, and the continuity equation, $\nabla\cdot\boldsymbol{u} = 0$, govern the fluid motion. Here, ρ_f and ν denote the mass density and kinematic viscosity of the fluid, respectively, and $\boldsymbol{f}(\boldsymbol{x},t)$ is an external body force. We consider the case that the particle is much smaller than the smallest eddies (i.e., the Kolmogorov length η) of turbulence and the volume fraction of particles is sufficiently small (say, smaller than 10^{-6}),[29,30] and therefore, the effect of the particles on the fluid motion is negligibly small.

We assume that particles are spherical, and their diameter D is small enough for the particle Reynolds number $\mathrm{Re}_p = D|\boldsymbol{v}_p - \boldsymbol{u}(\boldsymbol{x}_p)|/\nu$ to be sufficiently smaller than unity, where we denote the position and velocity of a particle by $\boldsymbol{x}_p$ and $\boldsymbol{v}_p$ $(= \mathrm{d}\boldsymbol{x}_p/\mathrm{d}t)$, respectively. We also

neglect the gravity and interactions between particles. Under these assumptions, Newton's equation of motion for a particle is expressed[31] by

$$\frac{\mathrm{d}\boldsymbol{v}_p}{\mathrm{d}t} = \beta \boldsymbol{a}(\boldsymbol{x}_p, t) - \frac{\boldsymbol{v}_p(t) - \boldsymbol{u}(\boldsymbol{x}_p, t)}{\tau_p}, \tag{1}$$

where $\boldsymbol{a}(\boldsymbol{x}, t)$ is the fluid acceleration. In (1),

$$\beta = 3/(2\gamma + 1), \tag{2}$$

where $\gamma = \rho_p/\rho_f$, with ρ_p being the particle mass density, is the added mass coefficient and

$$\tau_p = D^2/(12\beta\nu) \tag{3}$$

is the relaxation time of particle velocity. Note that the heavy- and light-particle limits correspond to $(\gamma, \beta) \to (\infty, 0)$ and (0, 3), respectively. Here, we define the non-dimensional relaxation time, namely, the Stokes number, by

$$\mathrm{St} = \tau_p/\tau_\eta, \tag{4}$$

where τ_η is the Kolmogorov time.

On the basis of (1), we develop a simple theoretical argument to clarify the condition for small particles (with arbitrary St and β) to form larger-scale clusters in turbulence. Our argument is similar to the classical one,[10,32] but we show that the argument is applicable to length scales larger than the Kolmogorov length η. Recall that larger voids of heavy particles are located at the positions of larger-scale vortices.[16] We will also show (see Figs. 1 and 3, below) that larger-scale clusters of light particles are formed around larger-scale vortices. Thus, in order to examine whether particles cluster by the action of vortices with size ℓ, we introduce an imaginary particle, with position $\boldsymbol{x}_c$ and velocity $\boldsymbol{v}_c$ (= $\mathrm{d}\boldsymbol{x}_c/\mathrm{d}t$), which obeys

$$\frac{\mathrm{d}\boldsymbol{v}_c}{\mathrm{d}t} = \beta \boldsymbol{a}_c(\boldsymbol{x}_c, t; \ell) - \frac{\boldsymbol{v}_c(t) - \boldsymbol{u}_c(\boldsymbol{x}_c, t; \ell)}{\tau_p}. \tag{5}$$

Here, $\boldsymbol{u}_c(\boldsymbol{x}, t; \ell)$ and $\boldsymbol{a}_c(\boldsymbol{x}, t; \ell)$ are the velocity and acceleration fields coarse-grained at scale ℓ. Note that (5) is the definition of $\boldsymbol{v}_c$ for arbitrary τ_p. Since smaller-scale vortices are advected by larger-scale ones, we may ignore the fluid motion smaller than ℓ when we consider particle clusters larger than ℓ. Therefore, we may assume that the imaginary particles governed by (5) reproduce the clusters, larger than ℓ, of real particles governed by (1). Under this assumption, which will be verified later in this article, we can examine their formation in terms of $\boldsymbol{x}_c$ and $\boldsymbol{v}_c$, instead of $\boldsymbol{x}_p$ and $\boldsymbol{v}_p$.

In practice, we estimate $\boldsymbol{u}_c$ by using the sharp low-pass filtering of the Fourier modes of $\boldsymbol{u}$ with the cutoff wavenumber $k_c = 2\pi/\ell$, whereas we define $\boldsymbol{a}_c$ by $-(1/\rho_f)\nabla p_c + \nu\nabla^2 \boldsymbol{u}_c + \boldsymbol{f}_c$. Here, $\boldsymbol{f}_c(\boldsymbol{x}, t; \ell)$ is the coarse-grained force and $p_c(\boldsymbol{x}, t; \ell)$ is the solution to the Poisson equation:

$$\nabla^2 p_c = -\rho_f \nabla \cdot [\boldsymbol{u}_c \cdot \nabla \boldsymbol{u}_c] = \rho_f Q_c, \tag{6}$$

where Q_c is the second invariant of the coarse-grained velocity gradient tensor $\nabla \boldsymbol{u}_c$.

Then, on the basis of (5), instead of (1), we can repeat the classical argument[10,32] for the relative velocity between the particle and fluid to obtain

$$\boldsymbol{v}_c - \boldsymbol{u}_c(\boldsymbol{x}_c, t; \ell) = \tau_p(\beta - 1)\boldsymbol{a}_c(\boldsymbol{x}_c, t; \ell). \tag{7}$$

Note that (7) holds when $\tau_p \ll T(\ell)$, where $T(\ell)$ is the eddy turnover time of size ℓ. In analogy with the turnover time $\mathscr{T}$ (i.e., the integral time) of the largest eddies, we define $T(\ell)$ by $\ell/u_c'(\ell)$, with $u_c'(\ell)$ being the root mean square of a component of the high-pass filtered velocity field at ℓ. In practice, we may estimate $T(\ell)$ by $\langle |Q_c(\ell)| \rangle^{-1/2}$, where $\langle \cdot \rangle$ denotes the spatiotemporal average because Q_c is predominantly determined by the smallest-scale (i.e., $\ell = 2\pi/k_c$) vortices in the coarse-grained field; see Ref. 33 for more detailed arguments.

If ℓ is a scale in the inertial range ($\eta \ll \ell \ll \mathscr{L}$), $\boldsymbol{a}_c \approx -(1/\rho_f)\nabla p_c$. Take the divergence of (7) and substitute this approximation and (6) into it to obtain

$$\nabla \cdot \boldsymbol{v}_c = -\tau_p(\beta - 1)Q_c, \tag{8}$$

which implies that blobs of light particles with $\beta > 1$ (or heavy particles with $\beta < 1$) tend to shrink in the region with $Q_c > 0$ (or $Q_c < 0$). Since $Q_c > 0$ (or $Q_c < 0$) means the dominance of the vorticity (or strain-rate) at scale ℓ, (8) implies the *tendency* that light particles accumulate around the axis of vortices with size ℓ, whereas heavy particles are swept out from them.

We derive the condition that particles form clusters with size ℓ by considering the contraction rate σ of particle blobs. First, note that (8) implies $\sigma = \tau_p(\beta - 1)Q_c$ (> 0). Since $|Q_c| \sim T(\ell)^{-2}$, $\sigma \sim \tau_p|1 - \beta|/T(\ell)^2$ and particle blobs with initial volume V_0 are contracted by eddies with size ℓ into the volume

$$V = V_0 \exp\left[-\sigma T^{\mathrm{life}}\right] = V_0 \exp\left[-|1 - \beta|S(\ell)K(\ell)\right], \tag{9}$$

during the mean lifetime[34] $T^{\mathrm{life}}(\ell)$ of eddies with size ℓ. In (9), $S(\ell) = \tau_p/T(\ell)$ and $K(\ell) = T^{\mathrm{life}}(\ell)/T(\ell)$ are the scale-dependent Stokes and Kubo numbers. From (9), the condition for particle clustering (i.e., $V \ll V_0$) is

$$|1 - \beta|S(\ell)\, K(\ell) \gtrsim 1. \tag{10}$$

Note that even when the scale-dependent Stokes number $S(\ell)$ is much smaller than 1, particles can form clusters with size ℓ if the lifetime $T^{\mathrm{life}}(\ell)$ (and therefore, $K(\ell)$) of scale-ℓ coherent structures is large so that (10) is satisfied.

Combining the validity condition of (7) (i.e., $\tau_p \lesssim T(\ell)$) and the contraction condition (10), we see that the clustering of particles occurs when the scale-dependent Stokes and Kubo numbers satisfy

$$\frac{1}{K(\ell)|1 - \beta|} \lesssim S(\ell) \lesssim 1. \tag{11}$$

This implies that particles with a given St may form clusters by the action of eddies with size ℓ when

$$\frac{1}{K(\ell)|1 - \beta|}\frac{T(\ell)}{\tau_\eta} \lesssim \mathrm{St} \lesssim \frac{T(\ell)}{\tau_\eta}. \tag{12}$$

This is the main result of the above argument, which gives the condition for particles to form scale-ℓ clusters. It is now clear that even when $\mathrm{St} \gg 1$, particles can form clusters. Incidentally, by using the Kolmogorov scaling $T(\ell) \sim \varepsilon^{-1/3}\ell^{2/3}$ in the inertial range, we can rewrite (12) as $[1/(K(\ell)|1 - \beta|)](\ell/\eta)^{2/3} \lesssim \mathrm{St} \lesssim (\ell/\eta)^{2/3}$. Hence, if $K(\ell) \approx 1$, the cluster size of particles, with τ_p being in the inertial time range ($\tau_\eta \ll \tau_p \ll \mathscr{T}$), would be $\ell \approx \mathrm{St}^{3/2}\eta$. However, as will be

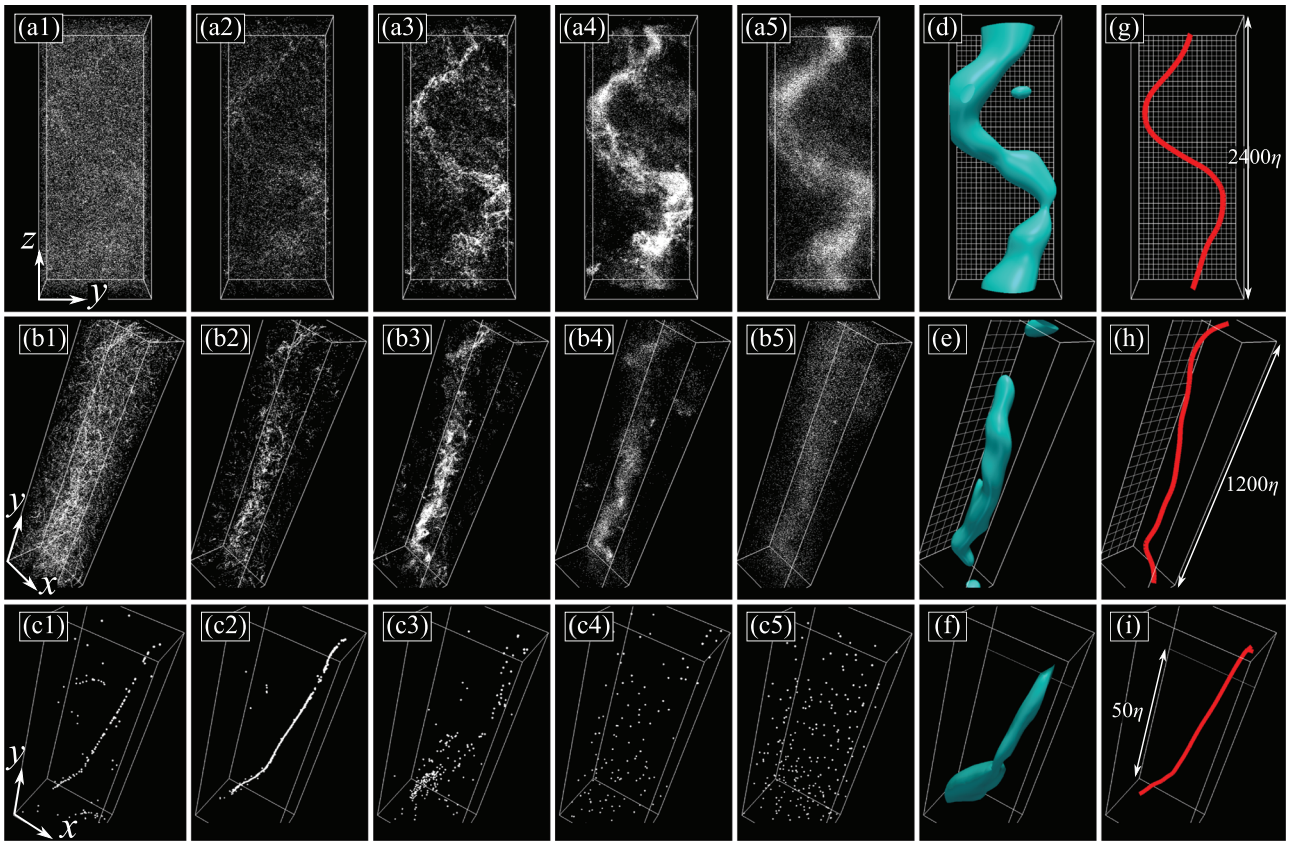

FIG. 1. (a)–(c) Spatial distribution of particles (white dots) with $\beta = 3$ and five different Stokes numbers: (a1)–(c1) St = 0.25, (a2)–(c2) 1, (a3)–(c3) 4, (a4)–(c4) 16, and (a5)–(c5) 64 in turbulence driven by the steady force. (d)–(f) Isosurfaces of the second invariant Q_c of the coarse-grained velocity gradient tensor at scale (d) 600η, (e) 150η, and (f) 9.4η. The threshold of isosurfaces is (d) $Q_c = \mu + s$, (e) $\mu + 4s$, and (f) $\mu + 0.6s$, where μ and s denote the spatial average and standard deviation of Q_c. (g)–(i) Vortex axes identified by applying the low-pressure method to coarse-grained turbulence, where the coarse-graining scale is the same as (d), (e), and (f), respectively. The size of the shown domain is [(a), (d), and (g)] $800\eta \times 1000\eta \times 2400\eta$, [(b), (e), and (h)] $300\eta \times 1200\eta \times 200\eta$, and [(c), (f), and (i)] $25\eta \times 65\eta \times 20\eta$. The grid width in (d), (e), (g), and (h) indicates 50η.

shown below, the clusters have multi-scale nature, which implies that coherent structures are rather robust, i.e., $K(\ell)$ can be sufficiently larger than 1.

Since the above argument reduces to the one for heavy particles in the limit of $\beta \to 0$ and since large-scale clusters of heavy particles were demonstrated in Refs. 16 and 18, here, we verify it for light particles ($\beta = 3$) in high-Reynolds number turbulence. For this purpose, we numerically simulate the motion of fluid and particles by simultaneously integrating the governing equations by the fourth-order Runge-Kutta-Gill scheme. We conduct DNSs with two different external forces: one is a steady force expressed by $\boldsymbol{f} = (-\sin x \cos y, +\cos x \sin y, 0)$ and the other is a random forcing imposed in a low-wavenumber range.[35] We evaluate the spatial derivatives in the governing equations for the fluid by the Fourier spectral method. We use $N^3 = 1024^3$ Fourier modes to simulate fully developed turbulence with the Taylor-length Reynolds number being $R_\lambda = 470$ by the steady force and $R_\lambda = 430$ by the random forcing. After statistically steady turbulence is realized, we distribute 256^3 particles, for each St, homogeneously in space, with their initial velocity being $\mathbf{0}$, and track them by integrating (1). We list the parameters and statistics of simulated turbulence in Table I. We simulate particle motions with eight different values of the Stokes number: St = 0.25, 1, 2, 4, 8, 16, 32, and 64; we take their statistics over the period $75\,\mathscr{T}$.

Figures 1(a)–1(c) show the spatial distribution of light particles ($\beta = 3$) with different values of St: (1) 0.25, (2) 1, (3) 4, (4) 16, and (5) 64 for the case of the steady force. The five panels in Figs. 1(a1)–1(a5) show the observation in a large domain ($800\eta \times 1000\eta \times 2400\eta$). We can observe clear clusters for St = 16 in this large scale [Fig. 1(a4)], whereas clusters in this scale are obscure for smaller Stokes numbers [St = 0.25 and 1 in Figs. 1(a1) and 1(a2)]. However, looking at a smaller scale [Fig. 1(c2); $100\eta \times 130\eta \times 50\eta$], the particles with St = 1 do form sharp curve-like clusters. This cluster is similar to the accumulation of particles in η-scale vortices in lower-Reynolds number turbulence.[36] It is also clear that for intermediate values of St (e.g., St = 4), particles form clusters in intermediate (but much larger than η) scales [see Fig. 1(b3), whose domain size is $300\eta \times 1200\eta \times 200\eta$]. These observations are consistent with the predictions of the above arguments; particles even with St $\gg 1$ can form clusters, and the clusters are larger for larger St. Incidentally, similar observations are made

TABLE I. Parameters and statistics of the simulated turbulence: N^3, the number of Fourier modes; R_λ, Taylor-length Reynolds number; L $(=2\pi)$, side of the periodic cube; $\mathscr{L}$, integral length; η, Kolmogorov length; $\mathscr{T}$ $(=\mathscr{L}/u')$, where u' is the root mean square of a component of the fluid velocity), integral time; τ_η, Kolmogorov time. The CFL number is defined by $u'\Delta t N/L$, where Δt is the time increment of the temporal integration.

Forcing	N^3	R_λ	$L/\mathscr{L}$	L/η	$\mathscr{L}/\eta$	$\mathscr{T}/\tau_\eta$	CFL
Steady	1024^3	470	5.6	2.4×10^3	430	39	6.9×10^{-2}
Random	1024^3	430	5.1	2.3×10^3	450	43	7.4×10^{-2}

also for the case of the random forcing. We will show the quantification and comparison between the two cases in Fig. 2.

The hierarchy of particle clusters observed in Fig. 1 [e.g., (a4), (b3), and (c2)] reflects the hierarchy of coherent vortices. We plot the isosurfaces of Q_c in Figs. 1(d)–1(f) for three different coarse-graining scales. It is striking that each cluster for different scales is spatially correlated with the coherent tubular vortex at different scales.

It is worth mentioning that since coherent vortices at a given scale tend to exist around larger ones,[25,37] particle clusters at different scales tend not to overlap. For example, we look at different locations in Figs. 1(a) and 1(b).

To objectively identify coherent tubular vortices at each level in the hierarchy of vortices, we apply the low-pressure method[38,39] to the coarse-grained pressure field.[26] We show the identified vortex axes in Figs. 1(g)–1(i) for the three different scales, namely, the largest scale

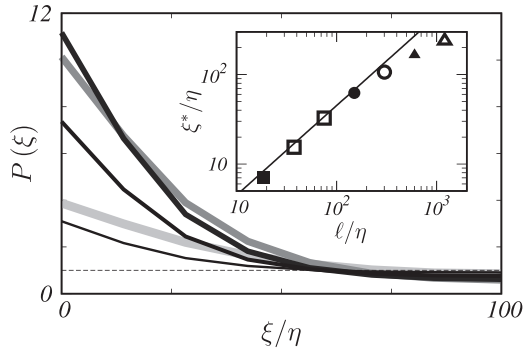

FIG. 3. Mean number density P of particles as a function of distance ξ from the nearest vortex axis with the coarse-graining scale $\ell = 150\eta$ in turbulence driven by the steady force. $P=1$ corresponds to the homogeneous distribution. Different curves are for different values of St from the thinner (and darker) to thicker (and lighter) lines, St = 0.25, 1, 4, 16, and 64. Average over 80 snapshots. The inset shows the thickness ξ^* of particle clusters, which is estimated by the condition $P(\xi^*) = 1$, as a function of ℓ. ■, St = 1; □, 2; ●, 4; ○, 8; ▲, 16; △, 32. The solid line indicates $\xi^* = 0.45\ell$.

$(\ell = 600\eta)$, the intermediate scale $(\ell = 150\eta)$, and the smallest scale $(\ell = 9.4\eta)$. Each vortex axis [Figs. 1(g)–1(i)] almost perfectly expresses the centerline of the particle clusters shown in Figs. 1(a4), 1(b3), and 1(c2). These results further support the arguments.

To quantify the observation in Fig. 1, we estimate the probability for the particles to exist inside vortices of size ℓ. Figure 2 shows the

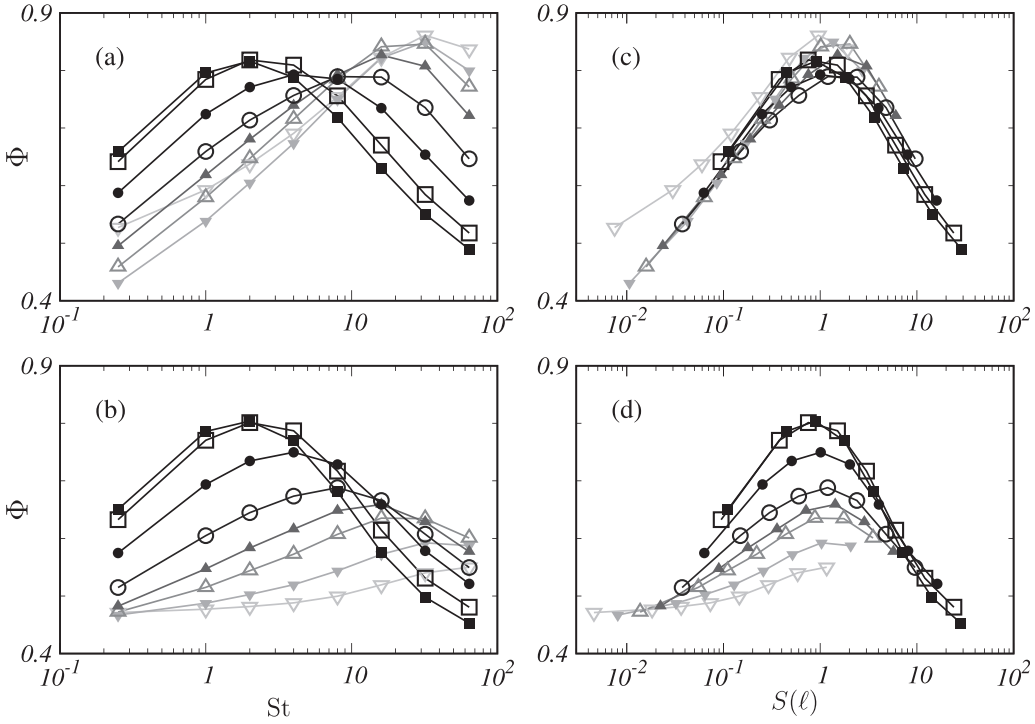

FIG. 2. Number ratio of particles in the vortical region ($Q_c > 0$) as functions of [(a) and (b)] St and [(c) and (d)] $S(\ell)$ in the turbulence driven by [(a) and (c)] the steady and [(b) and (d)] random forces. Different lines (lighter tone denotes larger ℓ) show the result for different scales: [(a) and (c)] ■, $\ell/\eta = 9.4$; □, 19; ●, 38; ○, 75; ▲, 150; △, 300; ▼, 600; ▽, 1200. [(b) and (d)] ■, $\ell/\eta = 8.9$; □, 18; ●, 35; ○, 71; ▲, 140; △, 280; ▼, 570; and ▽, 1100. We have taken the average over 20 snapshots.

number ratio Φ of particles in vortical regions with $Q_c(\boldsymbol{x}, t; \ell) > 0$, where $\Phi = 1$ (0) means that all (no) particles are in regions $Q_c > 0$. Note that the volume ratio of regions with $Q_c(\boldsymbol{x}, t; \ell) > 0$, in the simulated turbulence, is about 0.4 although it weakly depends on ℓ. Therefore, $\Phi > 0.4$ implies that particles are more likely to exist in vortical regions. We show the results for the steady forcing in Fig. 2(a) and for the random forcing in Fig. 2(b). Different curves show the results for different ℓ values. In both cases, we see that eddies with different sizes ℓ attract particles with different values of St. For example, looking at curves with ■ and □ [(a) $\ell = 9.4\eta$ and $\ell = 19\eta$; (b) $\ell = 8.9\eta$ and $\ell = 18\eta$], we see that particles with St = 2 are most attracted by these smallest-scale vortices. This result is consistent with the visualization in Fig. 1(c) and with the classical argument that light particles with St ≈ 1 most accumulate around the axes of Kolmogorov-scale vortices. It is also interesting that these curves seem universal irrespective of the kind of forcing.

Furthermore, we see that the value of St, which gives the peak of each curve in Figs. 2(a) and 2(b), monotonically increases with ℓ; note that the lighter tone denotes larger ℓ in Fig. 2. Again, this is consistent with the observations in Fig. 1, and it supports our arguments leading to (11). Figure 2 also shows that the largest-scale vortices [in Fig. 2(a) for $\ell = 1200\eta$ and in Fig. 2(b) for $\ell = 1100\eta$] attract particles with very large Stokes numbers (St = 32 or 64).

We may expect that $K(\ell)$ in the inertial range is independent of ℓ because of self-similarity. In such a simple case, the clustering condition (11) is expressed only by the scale-dependent Stokes number $S(\ell)$. To examine this, we replot Φ as a function of $S(\ell)$ in Figs. 2(c) and 2(d). Here, as mentioned below (7), we estimate $T(\ell)$ by $\langle |Q_c(\ell)| \rangle^{-1/2}$. In both cases, the peaks are located at $S(\ell) \approx 1$. This is a direct verification of our argument on the clustering condition.

Incidentally, the collapse of the curves in Fig. 2(c) may be coincidence; note that they are collapsed only in small scales for the random forcing [Fig. 2(d)].

Next, let us evaluate the size of particle clusters. Since we have identified the vortex axes by the low-pressure method, we may examine particle distributions around each axis. We evaluate the mean number density $P(\xi)$ of particles at distance ξ from the nearest vortex axis. We show the results in Fig. 3 for the case that the coarse-graining scale $\ell = 150\eta$, which corresponds to Figs. 1(b), 1(e), and 1(h). In Fig. 3, P is normalized so that $P = 1$ indicates the homogeneous distribution. The five curves in the figure show P for five different values of St. Note that $P(0)$ is largest for St = 4. This is consistent with the observation in Figs. 1(b), 1(e), and 1(h) that particles with St = 4 form the clearest clusters for the scale ($\ell = 150\eta$). We have also confirmed that $P(0)$ is largest when St = 16 and 1 in the case that $\ell = 600\eta$ and 9.4η, respectively. These are also consistent with the observations in Fig. 1.

By using the number-density distribution P, we may estimate the thickness ξ^* of particle clusters by the minimum value of ξ, which satisfies $P(\xi) = 1$ for St giving the maximum of $P(0)$. The inset of Fig. 3 shows ξ^* as a function of ℓ, which shows the proportionality $\xi^* = 0.45\ell$ in the range $\ell \leq 300\eta$. This is reasonable because of the self-similarity of coherent structures in the inertial range. The proportionality does not hold for the larger scales ($\ell = 600\eta$ and 1200η) because large-scale vortices are directly affected by the external force and they are not self-similar.

Before closing this article, we develop three discussions. First, we verify the assumption that is the starting point of our theoretical arguments; namely, if the real particles form clusters larger than ℓ, then the imaginary particles in the coarse-grained field governed by (5) also form the same clusters. We show in Fig. 4 the direct verification in two cases with different values of St. Figures 4(a) and 4(c) show the distributions of real and imaginary particles with St = 16, respectively. They form the same cluster for the scale $\ell = 600\eta$ although smaller clusters have different structures, i.e., we do not observe smaller clusters in Fig. 4(c). We can verify the assumption also for smaller St (= 4) as shown in Figs. 4(b) and 4(d). It is evident that the real and imaginary particles form the same cluster in the scale $\ell = 150\eta$.

Second, we emphasize that the particle clusters are not single-scale structures. Although Figs. 2(c) and 2(d) show that the timescale matching, i.e., $S(\ell) \approx 1$, is important to predict the size of clusters of particles with a given St, they also show that vortices of size ℓ attract particles in a rather wide range of $S(\ell)$, say, $0.1 \lesssim S(\ell) \lesssim 10$. In other words, particles with a given St are affected by vortices in a wide range of length scales. In fact, Φ for St = 4 in Fig. 2(a) is sufficiently larger than 0.4 (the value for the uniform distribution) for all the length scales examined (i.e., $9.4\eta < \ell < 1200\eta$). This is consistent with the observation in Figs. 1(a3), 1(b3), and 1(c3) that particles with St = 4 form clusters by the action of vortices with different sizes.[40]

This multi-scale nature is similar to the one for the cluster of heavy particles reported in the previous studies.[16,18,41,42] There are two causes for this. First, as discussed below (12), $K(\ell)$ can be large. In

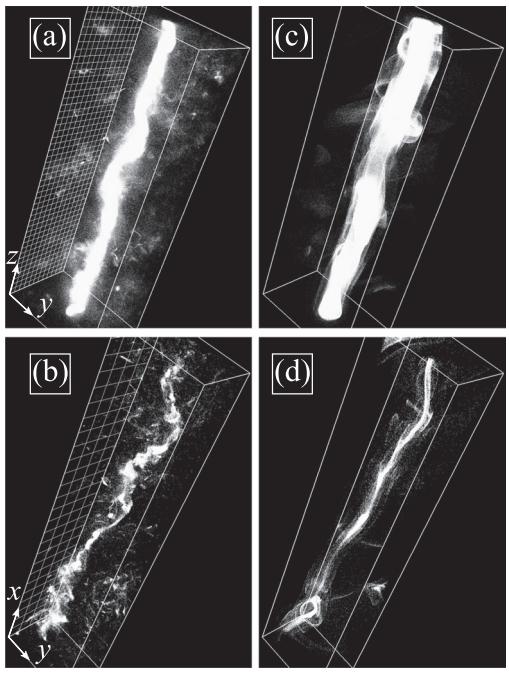

FIG. 4. Spatial distribution (white dots) of [(a) and (b)] the real and [(c) and (d)] imaginary particles with $\beta = 3$ and two different values of St: [(a) and (c)] St = 16 and [(b) and (d)] 4. The coarse-graining scale ℓ is (c) 600η and (d) 150η. The shown location and time are common in [(a) and (c)] and [(b) and (d)], respectively. The domain size is [(a) and (c)] $600\eta \times 850\eta \times 2400\eta$ and [(b) and (d)] $1300\eta \times 300\eta \times 200\eta$. Results for the turbulence driven by the steady force are shown. The grid width in (a) and (b) indicates 50η.

particular, in the case of the steady force, large-scale vortices have a long lifetime, and they affect particles with a wide range of St values. This gives the reason why clusters are observed even when $S(\ell)$ is much smaller than 1. The other cause is related to the upper bound of (11). More concretely, the above argument under the assumption $S(\ell) \lesssim 1$ is valid only when $\boldsymbol{v}_c$ is regarded as a field quantity and particles accumulate toward the axes of vortices with a swirling motion. However, even when $S(\ell)$ is larger than 1, but not too large, particles can oscillate around the axes of vortices.

The third discussion is on the identification of coherent vortices, which is a difficult task both in DNSs and experiments. Tracking light particles (with different values of St) is easier than the implementation of the low-pressure method to capture vortex axes (see Fig. 1) in DNSs. We may also suggest that if we appropriately choose the Stokes number of light particles, we can use them for the visualization of coherent vortices at different sizes in experiments. For example, in a typical experimental setup[43] of the von Kármán turbulence ($R_\lambda = 890$, $\mathscr{T} = 0.2$ s, and $\tau_\eta = 0.26$ ms), we may visualize the smallest- and largest-scale vortices by using silica aerogel particles (whose mass ratio to water is about 0.1;[44] i.e., $\beta \approx 2.5$), with diameter D being 90 μm and 2 mm, respectively.[45]

In conclusion, small particles with the added mass coefficient β, (2), and the Stokes number St, (4), form clusters of size ℓ in fully developed turbulence when condition (11), where $K(\ell)$ denotes the non-dimensionalized lifetime of coherent structures, is satisfied. This condition is consistent with the previous reports on the clustering of heavy particles.[16,18,28] To further verify the condition, we have conducted, for the first time, the DNSs of light particles with different Stoke numbers ($0.25 < \mathrm{St} < 64$) in turbulence at sufficiently high Reynolds numbers ($R_\lambda = 470$ and 430) for two different external forces; we have demonstrated that light particles accumulate around the axes of coherent vortices, whose size depends on St (Fig. 1). Condition (11) well explains the observations that the particle clusters are larger for larger St (Figs. 1 and 3) and they have multi-scale nature (Fig. 2), indicating the longevity of coherent structures.

This study was partly supported by JSPS Grants-in-Aids for Scientific Research (Nos. 16H04268 and 20H02068). The DNSs were conducted with the support of the NIFS Collaboration Research Programs (Nos. 18KNSS108 and 20KNSS145).

DATA AVAILABILITY

The data that support the findings of this study are available from the corresponding author upon reasonable request.

REFERENCES

[1]S. Balachandar and J. K. Eaton, "Turbulent dispersed multiphase flow," Annu. Rev. Fluid Mech. **42**, 111 (2010).
[2]K. Gustavsson and B. Mehlig, "Statistical models for spatial patterns of heavy particles in turbulence," Adv. Phys. **65**, 1 (2016).
[3]R. A. Shaw, "Particle-turbulence interactions in atmospheric clouds," Annu. Rev. Fluid Mech. **35**, 183 (2003).
[4]P. A. Vaillancourt and M. K. Yau, "Review of particle-turbulence interactions and consequences for cloud physics," Bull. Am. Met. Soc. **81**, 285 (2000).
[5]I. Saito and T. Gotoh, "Turbulence and cloud droplets in cumulus clouds," New J. Phys. **20**, 023001 (2018).
[6]J. N. Cuzzi, R. C. Hogan, J. M. Paque, and A. R. Dobrovolskis, "Size-selective concentration of chondrules and other small particles in protoplanetary nebula turbulence," Astrophys. J. **546**, 496 (2001).
[7]L. Pan, P. Padoan, J. Scalo, A. G. Kritsuk, and M. L. Norman, "Turbulent clustering of protoplanetary dust and planetesimal formation," Astrophys. J. **740**, 6 (2011).
[8]M. Colombini and A. Stocchino, "Ripple and dune formation in rivers," J. Fluid Mech. **673**, 121 (2011).
[9]F. Schuurman, W. A. Marra, and M. G. Kleinhans, "Physics-based modeling of large braided sand-bed rivers: Bar pattern formation, dynamics, and sensitivity," J. Geophys. Res. Earth Surf. **118**, 2509, https://doi.org/10.1002/2013JF002896 (2013).
[10]M. R. Maxey, "The gravitational settling of aerosol particles in homogeneous turbulence and random flow fields," J. Fluid Mech. **174**, 441 (1987).
[11]K. D. Squires and J. K. Eaton, "Particle response and turbulence modification in isotropic turbulence," Phys. Fluids A **2**, 1191 (1990).
[12]K. D. Squires and J. K. Eaton, "Preferential concentration of particles by turbulence," Phys. Fluids A **3**, 1169 (1991).
[13]L. P. Wang and M. R. Maxey, "Settling velocity and concentration distribution of heavy particles in homogeneous isotropic turbulence," J. Fluid Mech. **256**, 27 (1993).
[14]J. C. Sommerer and E. Ott, "Particles floating on a moving fluid: A dynamically comprehensible physical fractal," Science **259**, 335 (1993).
[15]J. Bec, L. Biferale, M. Cencini, A. Lanotte, S. Musacchio, and F. Toschi, "Heavy particle concentration in turbulence at dissipative and inertial scales," Phys. Rev. Lett. **98**, 084502 (2007).
[16]H. Yoshimoto and S. Goto, "Self-similar clustering of inertial particles in homogeneous turbulence," J. Fluid Mech. **577**, 275 (2007).
[17]S. Goto and J. C. Vassilicos, "Sweep-stick mechanism of heavy particle clustering in fluid turbulence," Phys. Rev. Lett. **100**, 054503 (2008).
[18]A. D. Bragg, P. J. Ireland, and L. R. Collins, "Mechanisms for the clustering of inertial particles in the inertial range of isotropic turbulence," Phys. Rev. E **92**, 023029 (2015).
[19]A. Crisanti, M. Falcioni, A. Provenzale, P. Tanga, and A. Vulpiani, "Dynamics of passively advected impurities in simple two-dimensional flow models," Phys. Fluids A **4**, 1805 (1992).
[20]M. Wilkinson and B. Mehlig, "Caustics in turbulent aerosols," Europhys. Lett. **71**, 186 (2005).
[21]S. Douady, Y. Couder, and M. E. Brachet, "Direct observation of the intermittency of intense vorticity filaments in turbulence," Phys. Rev. Lett. **67**, 983 (1991).
[22]J. Zhai, M. Fairweather, and M. Colombo, "Simulation of microbubble dynamics in turbulent channel flows," Flow Turbul. Combust. **105**, 1303 (2020).
[23]G. Shim, H. Park, S. Lee, and C. Lee, "Behavior of microbubbles in homogeneous stratified turbulence," Phys. Rev. Fluids **5**, 074302 (2020).
[24]F. Motta, F. Battista, and P. Gualtieri, "Application of the exact regularized point particle method (ERPP) to bubble laden turbulent shear flows in the two-way coupling regime," Phys. Fluids **32**, 105109 (2020).
[25]S. Goto, "A physical mechanism of the energy cascade in homogeneous isotropic turbulence," J. Fluid Mech. **605**, 355 (2008).
[26]S. Goto, Y. Saito, and G. Kawahara, "Hierarchy of antiparallel vortex tubes in spatially periodic turbulence at high Reynolds numbers," Phys. Rev. Fluids **2**, 064603 (2017).
[27]Y. Motoori and S. Goto, "Generation mechanism of a hierarchy of vortices in a turbulent boundary layer," J. Fluid Mech. **865**, 1085 (2019).
[28]S. Oka and S. Goto, "Generalized sweep-stick mechanism of inertial-particle clustering in turbulence," Phys. Rev. Fluids (in press).
[29]S. Elghobashi, "Particle-laden turbulent flows: Direct simulation and closure models," Appl. Sci. Res. **48**, 301 (1991).
[30]S. Elghobashi, "On predicting particle-laden turbulent flows," Appl. Sci. Res. **52**, 309 (1994).
[31]M. R. Maxey and J. J. Riley, "Equation of motion for a small rigid sphere in a nonuniform flow," Phys. Fluids **26**, 883 (1983).
[32]J. Ferry and S. Balachandar, "A fast eulerian method for disperse two-phase flow," Int. J. Multiphase Flow **27**, 1199 (2001).
[33]S. Goto, "Coherent structures and energy cascade in homogeneous turbulence," Prog. Theor. Phys. Suppl. **195**, 139 (2012).
[34]Turbulence is composed of the hierarchy of coherent vortices [e.g., Figs. 1(d)–1(f)]. Therefore, we can estimate the lifetime of each coherent vortex by identifying and tracking their axes [Figs. 1(g)–1(i)]. Then, T^{life} is evaluated by their average.

[35]We numerically integrate the equation for the Fourier components of the vorticity and impose the random forcing, by adding uniform white-in-time random numbers, on the modes with the magnitude of the wavenumber vector being smaller than 2.
[36]L. P. Wang and M. R. Maxey, "The motion of microbubbles in a forced isotropic and homogeneous turbulence," Appl. Sci. Res. **51**, 291 (1993).
[37]T. Leung, N. Swaminathan, and P. A. Davidson, "Geometry and interaction of structures in homogeneous isotropic turbulence," J. Fluid Mech. **710**, 453 (2012).
[38]H. Miura and S. Kida, "Identification of tubular vortices in turbulence," J. Phys. Soc. Jpn. **66**, 1331 (1997).
[39]S. Kida and H. Miura, "Swirl condition in low-pressure vortices," J. Phys. Soc. Jpn. **67**, 2166 (1998).
[40]If small-scale vortices were clustered in a larger-scale vortex, the statistics shown in Fig. 2 would be meaningless. However, this is not the case; see Refs. 25 and 26.
[41]G. Jin, G. W. He, and L. P. Wang, "Large-eddy simulation of turbulent collision of heavy particles in isotropic turbulence," Phys. Fluids **22**, 055106 (2010).
[42]T. Ariki, K. Yoshida, K. Matsuda, and K. Yoshimatsu, "Scale-similar clustering of heavy particles in the inertial range of turbulence," Phys. Rev. E **97**, 033109 (2018).
[43]E. W. Saw, P. Debue, D. Kuzzay, F. Daviaud, and B. Dubrulle, "On the universality of anomalous scaling exponents of structure functions in turbulent flows," J. Fluid Mech. **837**, 657 (2018).
[44]A. S. Dorcheh and M. H. Abbasi, "Silica aerogel; synthesis, properties and characterization," J. Mater. Process. Technol. **199**, 10 (2008).
[45]These particle diameters are determined by the conditions $\tau_p \approx \tau_\eta$ and $\tau_p \approx \mathscr{T}$, respectively. However, we may use smaller particles if the visualized vortices have a long lifetime. This is because, according to (11), vortices with scale ℓ are visualized by the particles with a diameter D in the range $\sqrt{12\beta\nu T(\ell)/K(\ell)} \lesssim D \lesssim \sqrt{12\beta\nu T(\ell)}$. Although the estimated D can be larger than η, (5), and therefore (11), may be valid for $D < \ell$ and $\tau_p \approx \mathscr{T}$.